

# Dynamics of immersed molecules in superfluids

Michael J. Quist\* and Veit Elser

*Department of Physics, Cornell University, Ithaca, New York 14850*

(Dated: November 5, 2018)

The dynamics of a molecule immersed in a superfluid medium are considered. Results are derived using a classical hydrodynamic approach followed by canonical quantization. The classical model, a rigid body immersed in incompressible fluid, permits a thorough analysis; its effective Hamiltonian generalizes the usual rigid-rotor Hamiltonian. In contrast to the free rigid rotor, the immersed body is shown to have chaotic dynamics. Quantization of the classical model leads to new and experimentally verifiable features. It is shown, for instance, that chiral molecules can behave as "quantum propellers": the rotational-translational coupling induced by the superfluid leads to a nonzero linear momentum in the ground state. Hydrogen peroxide is a strong candidate for experimental detection of this effect. The signature is a characteristic splitting of rotational absorption lines. The  $1_{01} \rightarrow 1_{10}$  line in hydrogen peroxide, for example, is predicted to split into three lines separated by as much as  $0.01 \text{ cm}^{-1}$ , which is about the experimental linewidth.

## I. INTRODUCTION

The dynamics of a molecule moving within a bulk superfluid medium are not expected to be too different from its dynamics in vacuum. Like the vacuum, an unbounded fluid is homogeneous and invariant with respect to continuous translations and rotations. Moreover, in the exotic case of superfluids, the very low level of excitation achieved at low temperatures implies that there is a vanishing set of modes with which the immersed molecule can interact. These expectations are borne out in the spectroscopy of single impurity molecules in  $^4\text{He}$  nanodroplets, where the superfluid medium has little effect on the rotational spectrum beyond modifying the molecular moments of inertia [2–4].

On the other hand, a low temperature superfluid medium is distinct from the nonrelativistic vacuum in that it lacks a basic symmetry: Galilean invariance. The superfluid condensate defines a preferred rest frame, an "ether" relative to which molecular velocities should be measured. This implies, in particular, that the energy-momentum relationship of molecules immersed in superfluids can deviate from a parabolic form. Of more interest spectroscopically, the presence of a preferred rest frame also gives rise to the possibility of couplings between linear and angular momenta that are strictly forbidden in an environment with Galilean invariance. Evidence of such couplings would provide one of the most direct experimental signatures of the superfluid medium.

This paper develops a simple and general theoretical framework for the rigid-body dynamics of a molecule immersed in a bosonic superfluid. The classical analysis of an immersed body, presented in Section II, shows that an incompressible fluid medium adds 11 parameters to the usual 4 parameters characterizing a free rigid body. As a result, an immersed body is typically chaotic. The classical model is quantized in Section III, and the quan-

tum Hamiltonian is discussed. The most interesting new feature is a term of the form  $\mathbf{p} \cdot \mathbf{J}$  which directly couples the linear momentum of the molecule to its angular momentum. This coupling requires chirality in the molecule, and corresponds intuitively to the action of a propeller. It fully lifts the usual  $(2J+1)$ -fold degeneracy of rigid-rotor states with angular momentum  $J$ , providing a clear spectroscopic signature of the superfluid-induced rotational-translational coupling. An unusual consequence is that the ground state acquires nonzero linear momentum. In Section IV, the magnitude of the rotational-translational coupling is estimated for the chiral molecules HOOH and FOOH. The predicted splitting of rotational absorption lines, at least for HOOH, is comparable to the resolution of current experiments. Finally, in Section V, the results are discussed in the context of related work.

## II. CLASSICAL MECHANICS OF AN IMMERSED RIGID BODY

We consider a rigid body immersed in unbounded, incompressible fluid of uniform density  $\rho_f$ . The body occupies a bounded, simply-connected volume  $V$  from which the fluid is excluded; the surface of this volume is denoted by  $\partial V$ . The velocity of the fluid is described by a potential  $\phi(\mathbf{x})$ , such that  $\mathbf{v}_f = -\nabla\phi$ , which satisfies  $\nabla^2\phi = 0$  inside the fluid volume and  $|\nabla\phi(\mathbf{x})| \rightarrow 0$  as  $|\mathbf{x}| \rightarrow \infty$ . On the moving surface  $\partial V$ , the fluid velocity also must satisfy  $(\mathbf{v}_f - \mathbf{v}_s) \cdot \mathbf{n} = 0$ , where  $\mathbf{n}$  is the surface normal and  $\mathbf{v}_s$  is the surface velocity. Our goal is to obtain a classical Hamiltonian for the immersed body which can be readily quantized. The classical problem is treated in many hydrodynamics texts (e.g., Ref. [5]), to which we refer the reader desiring greater detail.

We first choose an origin and coordinate axes fixed in the body; this defines the body frame. The origin of the body frame is at  $\mathbf{y}$  in the lab frame, and the body axes are rotated by  $\hat{\mathcal{R}}$  from the lab axes. The three components of  $\mathbf{y}$  and the three Euler angles needed to parametrize the matrix  $\hat{\mathcal{R}}$  completely specify the position of the body.

---

\*Electronic address: [mjq1@cornell.edu](mailto:mjq1@cornell.edu)

When  $\mathbf{y} = \mathbf{0}$  and  $\hat{\mathcal{R}} = \hat{\mathbf{1}}$ , the body and lab frames coincide, and the body is said to be in the reference position. Let  $E_t$  be the Euclidean transformation which moves the body from the reference position to its position at time  $t$ . Explicitly,

$$E_t : \mathbf{x} \mapsto \mathbf{y}(t) + \hat{\mathcal{R}}(t)\mathbf{x}. \quad (1)$$

The time-dependence of  $V$  is simply  $V_t = E_t V_0$ , where  $V_0$  is a fixed volume; similarly,  $\partial V_t = E_t \partial V_0$ . The lab-frame velocity of a point  $E_t \mathbf{x}$ , which is fixed in the body, is

$$\frac{d}{dt}(E_t \mathbf{x}) = \dot{\mathbf{y}} + \boldsymbol{\omega} \times (\hat{\mathcal{R}}\mathbf{x}), \quad (2)$$

where  $\boldsymbol{\omega}$  is the body's angular velocity. The velocity potential at a point  $\mathbf{x}$  which is fixed in the body frame,  $\phi'(\mathbf{x}) \equiv \phi(E_t \mathbf{x})$ , satisfies fairly simple equations:  $\nabla^2 \phi' = 0$  outside  $V_0$ ,  $|\nabla \phi'(\mathbf{x})| \rightarrow 0$  as  $|\mathbf{x}| \rightarrow \infty$ , and

$$\begin{aligned} \nabla \phi'(\mathbf{x}) \cdot \mathbf{n} &= -\left(\hat{\mathcal{R}}^T \mathbf{v}_s(E_t \mathbf{x})\right) \cdot \mathbf{n} \\ &= -\left(\hat{\mathcal{R}}^T \dot{\mathbf{y}} + (\hat{\mathcal{R}}^T \boldsymbol{\omega}) \times \mathbf{x}\right) \cdot \mathbf{n} \end{aligned} \quad (3)$$

for  $\mathbf{x}$  on the fixed surface  $\partial V_0$ , where the surface velocity was calculated using Eq. (2). Indeed, the equations for  $\phi'$  are linear, with inhomogeneous boundary conditions linear in  $\hat{\mathcal{R}}^T \dot{\mathbf{y}}$  and  $\hat{\mathcal{R}}^T \boldsymbol{\omega}$ . The velocity potential can therefore be expressed as a linear combination,

$$\phi'(\mathbf{x}) = -(\hat{\mathcal{R}}^T \dot{\mathbf{y}})_\mu \psi_\mu(\mathbf{x}) - (\hat{\mathcal{R}}^T \boldsymbol{\omega})_\mu \chi_\mu(\mathbf{x}), \quad (4)$$

where the harmonic functions  $\psi_\mu$  and  $\chi_\mu$  satisfy

$$\nabla \psi_\mu(\mathbf{x}) \cdot \mathbf{n} = \mathbf{e}_\mu \cdot \mathbf{n}, \quad (5a)$$

$$\nabla \chi_\mu(\mathbf{x}) \cdot \mathbf{n} = (\mathbf{e}_\mu \times \mathbf{x}) \cdot \mathbf{n} \quad (5b)$$

on  $\partial V_0$ . These six functions characterize the fluid response to the six independent motions of the body; they depend only on the shape of  $\partial V_0$ .

For a free rigid body, the Lagrangian is just the kinetic energy. When the body is immersed, this is augmented by the kinetic energy of the fluid:

$$\begin{aligned} \delta L &= \int_{V^c} d^3 x \frac{1}{2} \rho_f |\nabla \phi(\mathbf{x})|^2 \\ &= \int_{V_0^c} d^3 x \frac{1}{2} \rho_f |\nabla \phi'(\mathbf{x})|^2, \end{aligned} \quad (6)$$

where the second integral is over the fluid volume  $V_0^c$ , the complement of the body volume  $V_0$ . This is easy to evaluate using Eq. (4). The total Lagrangian, including the fluid contribution [Eq. (6)], then has the form

$$L = \frac{1}{2} (\dot{\mathbf{y}}^T \hat{\mathcal{R}} \quad \boldsymbol{\omega}^T \hat{\mathcal{R}}) \begin{pmatrix} \hat{M} & \hat{G} \\ \hat{G}^T & \hat{I} \end{pmatrix} \begin{pmatrix} \hat{\mathcal{R}}^T \dot{\mathbf{y}} \\ \hat{\mathcal{R}}^T \boldsymbol{\omega} \end{pmatrix}. \quad (7)$$

The mass tensor  $\hat{M}$ , the rotational-translational coupling tensor  $\hat{G}$ , and the inertia tensor  $\hat{I}$  can each be expressed

as a sum of rigid-body and fluid tensors:  $\hat{M} = \hat{M}^{(0)} + \delta \hat{M}$  and so on.

The rigid-body tensors are

$$M_{\mu\nu}^{(0)} = \int d^3 x \rho(\mathbf{x}) \delta_{\mu\nu}, \quad (8a)$$

$$G_{\mu\nu}^{(0)} = \int d^3 x \rho(\mathbf{x}) \epsilon_{\mu\nu\lambda} x_\lambda, \quad (8b)$$

$$I_{\mu\nu}^{(0)} = \int d^3 x \rho(\mathbf{x}) (|\mathbf{x}|^2 \delta_{\mu\nu} - x_\mu x_\nu), \quad (8c)$$

where  $\rho(\mathbf{x})$  is the body-frame mass density of the body. The expressions for  $\hat{M}^{(0)}$  and  $\hat{I}^{(0)}$  are the usual ones, and  $\hat{G}^{(0)}$  is typically made to vanish by choosing the body's center of mass as the origin of the body frame. The rigid-body Lagrangian then takes the familiar form

$$L^{(0)} = \frac{1}{2} \dot{\mathbf{y}}^T \hat{M}^{(0)} \dot{\mathbf{y}} + \frac{1}{2} \boldsymbol{\omega}^T \hat{\mathcal{R}} \hat{I}^{(0)} \hat{\mathcal{R}}^T \boldsymbol{\omega}. \quad (9)$$

The fluid tensors are

$$\delta M_{\mu\nu} = \int_{V_0^c} d^3 x \rho_f \nabla \psi_\mu(\mathbf{x}) \cdot \nabla \psi_\nu(\mathbf{x}), \quad (10a)$$

$$\delta G_{\mu\nu} = \int_{V_0^c} d^3 x \rho_f \nabla \psi_\mu(\mathbf{x}) \cdot \nabla \chi_\nu(\mathbf{x}), \quad (10b)$$

$$\delta I_{\mu\nu} = \int_{V_0^c} d^3 x \rho_f \nabla \chi_\mu(\mathbf{x}) \cdot \nabla \chi_\nu(\mathbf{x}). \quad (10c)$$

Note that the mass and inertia tensors  $\hat{M}$  and  $\hat{I}$  are symmetric, while the rotational-translational coupling  $\hat{G}$  has no obvious symmetry. In the most general case there are  $6 + 6 + 9 = 21$  parameters in the Lagrangian. We can place the body origin at a conveniently chosen point in the body, reducing this to 18. We can then rotate the body axes with respect to the body, leaving 15. By comparison, the free rigid rotor has 4 parameters.

The classical Hamiltonian follows from the Lagrangian [Eq. (7)]:

$$\mathcal{H} = \frac{1}{2} (\mathbf{p}^T \hat{\mathcal{R}} \quad \mathbf{J}^T \hat{\mathcal{R}}) \begin{pmatrix} \hat{M} & \hat{G} \\ \hat{G}^T & \hat{I} \end{pmatrix}^{-1} \begin{pmatrix} \hat{\mathcal{R}}^T \mathbf{p} \\ \hat{\mathcal{R}}^T \mathbf{J} \end{pmatrix}, \quad (11)$$

where  $\mathbf{p}$  is the linear momentum, canonically conjugate to  $\mathbf{y}$ , and  $\mathbf{J}$  is the angular momentum in the lab frame. The components of  $\mathbf{J}$  have Poisson brackets  $[J_\mu, J_\nu]_{\text{cl}} = \epsilon_{\mu\nu\lambda} J_\lambda$ . It is convenient also to work with  $\mathbf{J}' = \hat{\mathcal{R}}^T \mathbf{J}$  and  $\mathbf{p}' = \hat{\mathcal{R}}^T \mathbf{p}$ , the angular and linear momenta in the body frame, in terms of which the Hamiltonian is particularly simple. These variables have Poisson brackets  $[J'_\mu, J'_\nu]_{\text{cl}} = -\epsilon_{\mu\nu\lambda} J'_\lambda$  and  $[J'_\mu, p'_\nu]_{\text{cl}} = -\epsilon_{\mu\nu\lambda} p'_\lambda$ . The classical Poisson brackets relate to the quantum commutators in the usual way, as  $[A, B] = i[A, B]_{\text{cl}}$ .

To express Eq. (11) in a form more amenable to quantization, we first define new tensors  $\hat{\alpha}$ ,  $\hat{\beta}$ , and  $\hat{\gamma}$  through

$$\begin{pmatrix} \hat{\alpha} & \hat{\beta} \\ \hat{\beta}^T & \hat{\gamma} \end{pmatrix} \equiv \begin{pmatrix} \hat{M} & \hat{G} \\ \hat{G}^T & \hat{I} \end{pmatrix}^{-1}. \quad (12)$$

In the following section it is shown that the model can be quantized without complication provided that  $\hat{\beta}$  is symmetric. We can ensure that  $\hat{\beta}$  is in fact symmetric by choosing the body frame's origin correctly. For a free rigid body, the body's center of mass is the correct choice, but this is not true in general. The tensors  $\hat{\alpha}$  and  $\hat{\beta}$  transform in a particular way when the body origin is translated within the body ( $\hat{\gamma}$  is unchanged); we can use the transformation law to find the appropriate choice of origin. Specifically, consider shifting the body origin by  $\mathbf{d}$ , so that all body-frame coordinates transform as  $\mathbf{x} \mapsto \mathbf{x} - \mathbf{d}$ . Then a direct calculation from Eqs. (8) shows that the rigid-body tensors transform as

$$\begin{pmatrix} \hat{M}^{(0)} & \hat{G}^{(0)} \\ \hat{G}^{(0)T} & \hat{I}^{(0)} \end{pmatrix} \mapsto \begin{pmatrix} \hat{\mathbf{1}} & 0 \\ \epsilon \mathbf{d} & \hat{\mathbf{1}} \end{pmatrix} \begin{pmatrix} \hat{M}^{(0)} & \hat{G}^{(0)} \\ \hat{G}^{(0)T} & \hat{I}^{(0)} \end{pmatrix} \begin{pmatrix} \hat{\mathbf{1}} & -\epsilon \mathbf{d} \\ 0 & \hat{\mathbf{1}} \end{pmatrix}, \quad (13)$$

where the antisymmetric matrix  $\epsilon \mathbf{d}$  has matrix elements  $(\epsilon \mathbf{d})_{\mu\nu} = \epsilon_{\mu\nu\lambda} d_\lambda$ . It is not hard to see that the fluid tensors transform in exactly the same way. Inverting the relation, we find that  $\hat{\beta} \mapsto \hat{\beta} + (\epsilon \mathbf{d})\hat{\gamma}$ . Now, the vector  $\mathbf{b}$  with components  $b_\lambda = \epsilon_{\mu\nu\lambda}\beta_{\mu\nu}$  is the zero vector exactly when  $\hat{\beta}$  is symmetric, and it transforms as  $\mathbf{b} \mapsto \mathbf{b} + \{(\text{Tr}\hat{\gamma})\hat{\mathbf{1}} - \hat{\gamma}\}\mathbf{d}$ . The matrix multiplying  $\mathbf{d}$  is positive definite, because  $\hat{\gamma}$  is, so it can be inverted. The result is that if  $\hat{\beta}$  is not symmetric, it can be made so by shifting the origin of the body frame by  $\mathbf{d} = -\{(\text{Tr}\hat{\gamma})\hat{\mathbf{1}} - \hat{\gamma}\}^{-1}\mathbf{b}$  within the body. We will assume that this has been done.

With the body origin fixed, rotation of the body axes can be used to diagonalize  $\hat{\gamma}$ , leaving it in the form  $\hat{\gamma} = \text{diag}(2A, 2B, 2C)$ . (Since  $\hat{\beta}$  transforms as a tensor under rotation, it will remain symmetric.) Note that  $A$ ,  $B$ , and  $C$  are *effective* rotational constants, shifted from their rigid-body values by the body's interaction with the fluid. Finally, the symmetric matrices  $\hat{\alpha}$  and  $\hat{\beta}$  can be broken down into their scalar and rank-2 spherical tensor components:

$$\hat{\alpha} = \alpha_0^{(0)}\hat{\mathbf{1}} + \sum_{q=-2}^2 \alpha_q^{(2)}\hat{\mathcal{M}}_q^{(2)}, \quad (14)$$

and analogously for  $\hat{\beta}$ , where

$$\hat{\mathcal{M}}_0^{(2)} = \frac{1}{\sqrt{6}} \begin{pmatrix} -1 & & \\ & -1 & \\ & & 2 \end{pmatrix}, \quad \hat{\mathcal{M}}_{\pm 1}^{(2)} = -\frac{1}{2} \begin{pmatrix} 0 & 0 & \pm 1 \\ 0 & 0 & i \\ \pm 1 & i & 0 \end{pmatrix},$$

$$\hat{\mathcal{M}}_{\pm 2}^{(2)} = \frac{1}{2} \begin{pmatrix} 1 & \pm i & 0 \\ \pm i & -1 & 0 \\ 0 & 0 & 0 \end{pmatrix}. \quad (15)$$

These matrices are defined to have nice rotational properties; in particular,

$$\hat{\mathcal{R}}\hat{\mathcal{M}}_q^{(2)}\hat{\mathcal{R}}^T = \sum_p \hat{\mathcal{M}}_p^{(2)}\mathcal{D}_{pq}^{(2)}, \quad (16)$$

where the  $\mathcal{D}_{pq}^{(2)}$  are rotation matrices, given by known functions of the Euler angles [6]. The Hamiltonian then has the form

$$\mathcal{H} = \frac{1}{2}\alpha_0^{(0)}p^2 + \beta_0^{(0)}\mathbf{p} \cdot \mathbf{J} + \mathcal{H}_{rr}(A, B, C) + \sum_q \frac{1}{2}\alpha_q^{(2)}\Pi_q^{(2)} + \sum_q \beta_q^{(2)}\Theta_q^{(2)}, \quad (17)$$

where  $\mathcal{H}_{rr}$  is the rigid rotor Hamiltonian,

$$\mathcal{H}_{rr}(A, B, C) = AJ_x'^2 + BJ_y'^2 + CJ_z'^2, \quad (18)$$

and  $\Pi^{(2)}$  and  $\Theta^{(2)}$  are spherical tensors of rank 2, with components

$$\Pi_q^{(2)} = (\mathbf{p}')^T \hat{\mathcal{M}}_q^{(2)} \mathbf{p}'; \quad \Theta_q^{(2)} = (\mathbf{p}')^T \hat{\mathcal{M}}_q^{(2)} \mathbf{J}'. \quad (19)$$

More precisely,  $\Pi^{(2)}$  and  $\Theta^{(2)}$  transform as spherical tensors of rank 2 under rotations generated by  $-\mathbf{J}'$ .

Before proceeding to the quantum case, we consider the classical dynamics of the model. The Lagrangian is invariant under arbitrary translations ( $\mathbf{y} \mapsto \mathbf{y} + \mathbf{a}$ ) and system rotations ( $\mathbf{y} \mapsto \hat{\mathcal{O}}\mathbf{y}$ ,  $\hat{\mathcal{R}} \mapsto \hat{\mathcal{O}}\hat{\mathcal{R}}$ ), but not under body rotations ( $\hat{\mathcal{R}} \mapsto \hat{\mathcal{O}}\hat{\mathcal{R}}$ ) alone. Therefore  $\mathbf{p}$  and the total (spin plus orbital) angular momentum  $\mathbf{J} + \mathbf{y} \times \mathbf{p}$  are constants of the motion, but  $\mathbf{J}$  is not, in contrast to the free rigid rotor. We can use these symmetries to simplify the system. Four constants of the motion, which have vanishing Poisson brackets with  $\mathcal{H}$  and with each other, are  $\mathbf{p} \cdot \mathbf{J}$  and the components of  $\mathbf{p}$ . By fixing these constants and eliminating the coordinates which are conjugate to them (the components of  $\mathbf{y}$  and one of the three Euler angles), we restrict the Hamiltonian to a reduced phase space; the equations of motion for the remaining degrees of freedom are unchanged by the reduction. In this case, the original six degrees of freedom are reduced to two, so the reduced phase space is four-dimensional. It can be parametrized by the directions of  $\mathbf{p}'$  and  $\mathbf{J}'$ , expressed in polar coordinates by the four angles  $(\theta_p, \phi_p, \theta_J, \phi_J)$ . The energy shells of the reduced phase space (i.e., the level sets of  $\mathcal{H}$ ) are three-dimensional.

The integrability of a Hamiltonian system with two degrees of freedom can be ascertained using a Poincaré section, essentially by inspection. To illustrate that the immersed rigid body is generally chaotic, we display a Poincaré section of the reduced phase space in Fig. 1. The figure was generated by repeatedly integrating the equations of motion, starting at many different points within the  $\mathcal{H} = 2$  energy shell, and plotting the point  $(\phi_J, \cos\theta_J)$  each time a trajectory crossed the plane  $\theta_p = \pi/2$ . The Hamiltonian parameters were  $\hat{\alpha} = \hat{\mathbf{1}}$ ,  $\hat{\beta} = \text{diag}(1, 1, -2)$ , and  $\hat{\gamma} = \text{diag}(1, 2, \sqrt{5})$ ; the conserved quantities were set to  $\mathbf{p} \cdot \mathbf{J} = 0.1$  and  $\mathbf{p} = 0.1\mathbf{e}_z$ . If the system were integrable, each phase space trajectory would be confined to a two-dimensional torus, and would appear in the figure as a densely dotted curve.

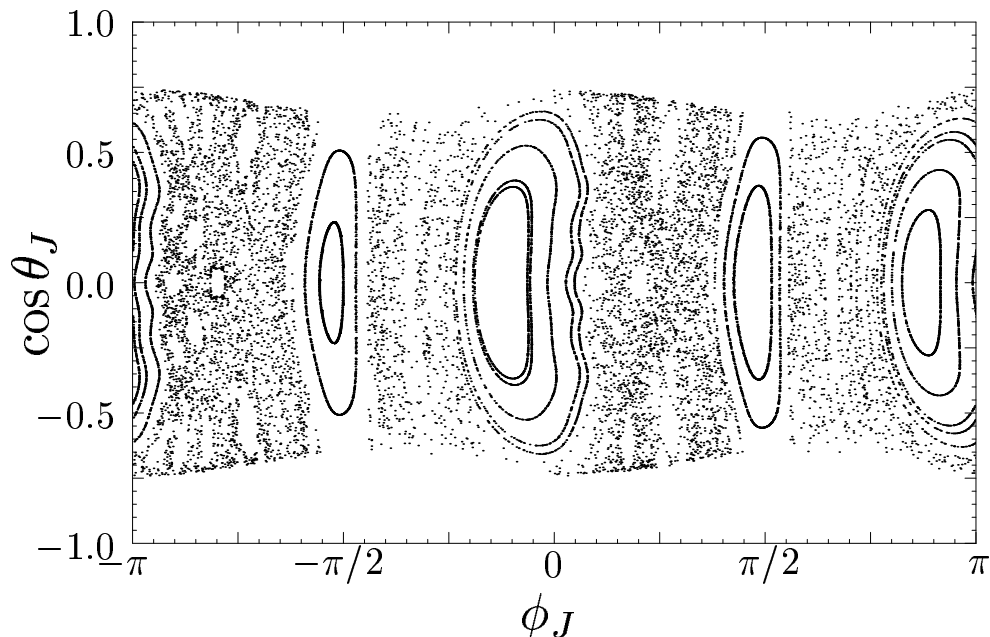


FIG. 1: Poincaré section of the reduced phase space of an immersed body, showing both chaotic and quasi-integrable regions.

Instead, the figure shows that the phase space contains chaotic regions, where trajectories ergodically visit three-dimensional volumes, as well as quasi-integrable regions, where trajectories are confined to two-dimensional tori. It should be noted that this set of parameter values corresponds to very strong coupling between linear and angular momenta, and was chosen to highlight the presence

of chaos. The physical cases we will consider in this paper are much more nearly integrable. Nevertheless, the existence of classical chaos suggests that the quantum spectrum, unlike that of the free rigid rotor, cannot be determined algebraically. We will need to use an approximate method, in this case a perturbative expansion in powers of the linear momentum.

### III. QUANTUM HAMILTONIAN

The quantization of the classical Hamiltonian [Eq. (17)] is straightforward, and proceeds as in any standard angular momentum text (see, for instance, Ref. [6]). There is only one subtlety. Since  $\mathbf{p}'$  and  $\mathbf{J}'$  have a nonvanishing Poisson bracket, their quantum counterparts do not commute, and the quantization of terms like  $p'_\mu J'_\nu$  suffers from an ordering ambiguity. We can sidestep this problem because we only need to quantize the components of  $\Theta^{(2)}$ : since  $[J'_\mu, p'_\nu]_{\text{cl}}$  is  $\mu\nu$ -antisymmetric, while each matrix  $\hat{\mathcal{M}}_q^{(2)}$  is symmetric, the operators  $\Theta_q^{(2)}$  are independent of the relative ordering of  $\mathbf{p}'$  and  $\mathbf{J}'$ . For the remainder of the paper,  $\mathbf{p}$ ,  $\mathcal{H}$ , etc., will refer to the appropriate quantum operators (or their eigenvalues) unless otherwise noted.

Breaking the Hamiltonian down into  $\mathcal{H}_0$  and  $\delta\mathcal{H}$ , respectively the first three and last two terms of Eq. (17), allows us to proceed perturbatively. Since  $\delta\mathcal{H}$  vanishes

for a free rigid rotor, this separates out the effects of the fluid. The  $\mathbf{p} \cdot \mathbf{J}$  term also is absent for a free rotor, but this term commutes with  $p^2$  and  $\mathcal{H}_{rr}$ , so it can be treated exactly.

Because  $\mathbf{p}$  is conserved, we can fix  $\mathbf{p} = k\mathbf{e}_z$ ,  $k \geq 0$ , with no loss of generality. A convenient basis for the remaining (angular) degrees of freedom is the set of simultaneous eigenvectors of  $J^2$ ,  $J'_z$ , and  $J_z$ ; the eigenvector with respective eigenvalues  $J(J+1)$ ,  $K$ , and  $M$  is denoted by  $|JKM\rangle$ . The tensor operators [Eq. (19)] become

$$\Pi_q^{(2)} = \frac{2}{\sqrt{6}} k^2 \mathcal{D}_{0q}^{(2)}, \quad (20a)$$

$$\Theta_q^{(2)} = k \left( \frac{1}{2} J_- \mathcal{D}_{-1q}^{(2)} + \frac{2}{\sqrt{6}} J_z \mathcal{D}_{0q}^{(2)} - \frac{1}{2} J_+ \mathcal{D}_{1q}^{(2)} \right), \quad (20b)$$

where  $J_\pm \equiv J_x \pm iJ_y$ . Their matrix elements are expressible in terms of Wigner 3- $j$  symbols [6]:

$$\begin{aligned}
\langle J_2 K_2 M_2 | \Pi_q^{(2)} | J_1 K_1 M_1 \rangle &= \frac{2}{\sqrt{6}} k^2 (-1)^{K_1+M_1} \sqrt{(2J_2+1)(2J_1+1)} \begin{pmatrix} J_2 & 2 & J_1 \\ K_2 & q & -K_1 \end{pmatrix} \begin{pmatrix} J_2 & 2 & J_1 \\ M_2 & 0 & -M_1 \end{pmatrix} \\
&= (-1)^{K_1} \begin{pmatrix} J_2 & 2 & J_1 \\ K_2 & q & -K_1 \end{pmatrix} \langle J_2 M_2 || \Pi^{(2)} || J_1 M_1 \rangle,
\end{aligned} \tag{21a}$$

and

$$\begin{aligned}
\langle J_2 K_2 M_2 | \Theta_q^{(2)} | J_1 K_1 M_1 \rangle &= k (-1)^{K_1+M_1} \sqrt{(2J_2+1)(2J_1+1)} \begin{pmatrix} J_2 & 2 & J_1 \\ K_2 & q & -K_1 \end{pmatrix} \times \\
&\quad \left\{ \frac{1}{2} \sqrt{(J_2-M_2)(J_2+M_2+1)} \begin{pmatrix} J_2 & 2 & J_1 \\ M_2+1 & -1 & -M_1 \end{pmatrix} + \frac{2M_2}{\sqrt{6}} \begin{pmatrix} J_2 & 2 & J_1 \\ M_2 & 0 & -M_1 \end{pmatrix} \right. \\
&\quad \left. - \frac{1}{2} \sqrt{(J_2-M_2+1)(J_2+M_2)} \begin{pmatrix} J_2 & 2 & J_1 \\ M_2-1 & 1 & -M_1 \end{pmatrix} \right\} \\
&= (-1)^{K_1} \begin{pmatrix} J_2 & 2 & J_1 \\ K_2 & q & -K_1 \end{pmatrix} \langle J_2 M_2 || \Theta^{(2)} || J_1 M_1 \rangle.
\end{aligned} \tag{21b}$$

The simple dependence of the matrix elements on  $K_1$ ,  $K_2$  and  $q$  is a consequence of the tensorial nature of the operators, and is guaranteed by the Wigner-Eckart theorem. The reduced matrix elements vanish unless  $M_2 = M_1$ , by inspection, so  $J_z$  commutes with both  $\mathcal{H}_0$  and  $\delta\mathcal{H}$ . This is to be expected from the classical conservation of  $\mathbf{p} \cdot \mathbf{J}$ , which equals  $kJ_z$  for our choice of  $\mathbf{p}$ .

The eigenvectors of  $\mathcal{H}_0$  are the simultaneous eigenvectors of the rigid rotor Hamiltonian and  $J_z$ . Since  $\mathcal{H}_{rr}$  can be written in a normalized form,

$$\mathcal{H}_{rr}(A, B, C) = \frac{1}{2}(A+C)J^2 + \frac{1}{2}(A-C)\mathcal{H}_{rr}(1, \kappa, -1), \tag{22}$$

the eigenvectors depend only on the asymmetry parameter  $\kappa = (-A+2B-C)/(A-C)$ . The eigenstates evolve continuously with  $\kappa$ ; they become eigenstates of  $J'_x$  and  $J'_z$  in the prolate ( $\kappa \rightarrow -1$ ) and oblate ( $\kappa \rightarrow 1$ ) limits respectively, with corresponding eigenvalues  $K_{-1}$  and  $K_{+1}$ . Following standard notation, we denote these states as  $|\tau M\rangle$ , where  $\tau \in \{J_{K_{-1}K_{+1}}\} = \{0_{00}, 1_{01}, 1_{11}, 1_{10}, \dots\}$  indicates both the angular momentum and the two limiting values of  $K$ , and  $M$  is the eigenvalue of  $J_z$ . The unperturbed energies are

$$\begin{aligned}
E_{\tau M}^{(0)} &= \frac{1}{2}\alpha_0^{(0)}k^2 + \beta_0^{(0)}Mk + \frac{1}{2}(A+C)J(J+1) \\
&\quad + \frac{1}{2}(A-C)\mathcal{E}_\tau(\kappa),
\end{aligned} \tag{23}$$

written in terms of the normalized rigid rotor eigenvalues  $\mathcal{E}_\tau(\kappa)$ .

We are now in a position to find the perturbed energies to any order in  $\delta\mathcal{H}$ . The expansion can be reordered as an expansion in the momentum  $k$ . The first-order correction comes from the diagonal elements of  $\Theta^{(2)}$ , which turn out to be proportional to  $M$  for each  $\tau$ . A given level has

energy

$$\begin{aligned}
E_{\tau M}(k) &= \frac{1}{2}(A+C)J(J+1) + \frac{1}{2}(A-C)\mathcal{E}_\tau(\kappa) \\
&\quad + \tilde{B}_\tau Mk + \frac{1}{2}\tilde{A}_{\tau M}k^2 + O(k^3),
\end{aligned} \tag{24}$$

where  $\tilde{B}_\tau$  and  $\tilde{A}_{\tau M}$  are calculated from matrix elements of  $\delta\mathcal{H}$  in the usual way. In particular,

$$\begin{aligned}
\tilde{B}_\tau &= \beta_0^{(0)} + \frac{1}{Mk} \sum_q \beta_q^{(2)} \left( \Theta_q^{(2)} \right)_{\tau\tau M}, \\
\tilde{A}_{\tau M} &= \alpha_0^{(0)} + \frac{1}{k^2} \sum_q \alpha_q^{(2)} \left( \Pi_q^{(2)} \right)_{\tau\tau M} \\
&\quad + \frac{2}{k^2} \sum_{q,q'} \beta_{q'}^{(2)} \beta_q^{(2)} \sum_{\tau'} \frac{\left( \Theta_{q'}^{(2)} \right)_{\tau\tau' M} \left( \Theta_q^{(2)} \right)_{\tau'\tau M}}{E_{\tau M}^{(0)} - E_{\tau' M}^{(0)}},
\end{aligned} \tag{25a}$$

where  $(\Theta)_{\tau\tau' M}$  is shorthand for  $\langle \tau M | \Theta | \tau' M \rangle$ . Higher-order terms are suppressed by additional factors of  $k\beta_q^{(2)}$  or  $k^2\alpha_q^{(2)}$ ; for the cases we consider in the next section, these factors are less than  $10^{-3}$ , so it is reasonable to truncate the expansion here. Clearly  $\tilde{A}_{\tau M}^{-1}$  is an effective mass; it reduces to the mass of the body in the absence of the fluid. The constant  $\tilde{B}_\tau$  is a pseudoscalar associated with the family of levels  $|\tau M\rangle$ . It is nonzero only in the presence of the fluid, and only when the immersed body is *chiral*. Judging from the spectrum,  $\tilde{B}_\tau$  measures the tendency of the immersed body to have its linear and angular momenta aligned. When this tendency is strong, the body behaves as a kind of ‘‘quantum propeller.’’

#### IV. MOLECULAR SURFACE MODEL AND NUMERICAL RESULTS

In order to apply these results to a real system, we must specify the fluid density  $\rho_f$ , model the surface  $\partial V_0$  and mass density  $\rho(\mathbf{x})$  which characterize the immersed body, and calculate the tensors  $\hat{M}$ ,  $\hat{G}$ , and  $\hat{I}$  from these inputs. In this section we consider the interesting case of an immersed *molecule* in superfluid helium. The fluid density  $\rho_f$  is approximately  $0.1 \text{ amu-}\text{\AA}^{-3}$ . The mass density of the molecule can be represented as  $\rho(\mathbf{x}) = \sum_i m_i \delta(\mathbf{x} - \mathbf{x}_i)$ , where the atomic coordinates  $\mathbf{x}_i$  are known. Helium is kept away from the molecule primarily by the short-ranged Fermi repulsion between molecular electrons and helium electrons. This results in a smoothly varying helium density, interpolating from zero near the molecule to  $\rho_f$  far away. Our model approximates this smooth variation by a discontinuous jump, localized on the imaginary surface  $\partial V_0$ . The optimal choice of surface is not obvious, but some criteria are clearly important. The surface should share the symmetries of the molecule; it should be smooth, since the electronic densities are smooth; and its size and shape should be physically reasonable: when compared to the actual helium density profile, the surface should approximate the surface  $\rho = \frac{1}{2}\rho_f$ . With these criteria in mind, we model the surface  $\partial V_0$  for an immersed molecule in the following way. First, we place a sphere of radius  $R_i$  at each atomic coordinate  $\mathbf{x}_i$ . Each radius is proportional to the van der Waals distance between a helium atom and an atom of type  $i$ :  $R_i = cR_{\text{He-}i}$ , where the parameter  $c$  will be of order 1. (For our calculations, we used  $R_{\text{He-H}} = 2.60 \text{ \AA}$ ,  $R_{\text{He-F}} = 2.87 \text{ \AA}$ , and  $R_{\text{He-O}} = 2.92 \text{ \AA}$  [7].) The union of these spheres forms a cuspy volume. The surface radius of the body volume, relative to an origin within the molecule, is represented in polar coordinates as  $r_s(\theta, \phi)$ . We then smooth the function  $r_s$  using the rotationally invariant linear operator which maps  $Y_{lm}(\theta, \phi) \mapsto \exp(-\alpha l) Y_{lm}(\theta, \phi)$ , with  $\alpha = 0.1$ , to yield the final surface  $\partial V_0$ . (Many other smoothing operators would do as well; our results are not very sensitive to the choice.) This prescription gives a single-parameter family of smooth surfaces which share the symmetry of the molecule; the parameter  $c$  can be adjusted to exclude superfluid from an appropriately sized volume.

Once the surface is fixed, the fluid tensors can be calculated either numerically or analytically. We used a perturbative analytical method, valid for nearly spherical surfaces, where the surface radius is a weakly varying function of polar angle:  $r_s(\theta, \phi) = r_0(1 + \epsilon(\theta, \phi))$ , with  $\epsilon \ll 1$ . The fluid response functions  $\psi_\mu$  and  $\chi_\mu$  (see Section II) can then be calculated as power series in  $\epsilon$ , as can the fluid contributions to the tensors. This calculation has been carried through to second order, which is the lowest order at which nontrivial rotational-translational coupling (i.e. a nonzero value for  $\tilde{B}_\tau$ ) is seen. The calculation and results are described in the Appendix.

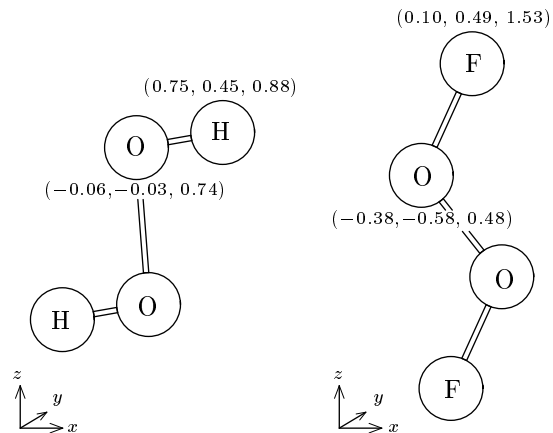


FIG. 2: Structures of the chiral molecules HOOH and FOOF. Atomic coordinates ( $x, y, z$ ) are shown, in  $\text{\AA}$ , for two atoms in each molecule. The undisplayed coordinates are obtained from these by a symmetry transformation,  $R_y(\pi) : (x, y, z) \mapsto (-x, y, -z)$ .

We present data for the low-lying levels of two different molecules: hydrogen peroxide (HOOH) and dioxygen difluoride (FOOF). These molecules are depicted in Fig. 2, with structural parameters taken from Ref. [8]. Each has a  $C_2$  point group, which we have taken to be  $C_2(y)$  by an appropriate rotation of body axes. The allowed rotational levels all have the same parity under rotation by  $\pi$  around the  $y$ -axis: either even ( $0_{00}, 1_{11}, 2_{02}, \dots$ ) or odd ( $1_{01}, 1_{10}, 2_{12}, \dots$ ), depending on the symmetry of the joint electronic/nuclear wavefunction. In the case where allowed levels are odd, the  $J = 0$  state is forbidden, so the ground state of the immersed molecule has  $J = 1$ , and, by Eq. (24), a nonzero linear momentum. The ground state momentum is  $k_0 = |\tilde{B}_{\tau_0}/\tilde{A}_{\tau_0,+1}|$ , where  $\tau_0$  is the ground state with  $J = 1$ .

The results for HOOH and FOOF are presented in Tables I and II respectively. (Energies are given in  $\text{cm}^{-1}$  or K; these conversions are made using  $k_B = hc = 1$ , consistent with usual spectroscopic notation. Momenta are given in  $\text{\AA}^{-1}$ ; this conversion is made using  $\hbar = 1$ .) The surfaces considered can be parametrized by their mean radius  $r_0$ , shown in the first column. The values displayed correspond to the parameter range  $0.5 \leq c \leq 1.5$  for each molecule. Although the inverse effective masses  $\tilde{A}_{\tau M}$  are level-dependent, this dependence is very weak, and  $\tilde{A}_{\tau M} \approx \alpha_0^{(0)}$  for the tabulated cases. This approximate value is displayed, as  $\tilde{A}$ , in the second column. The remaining columns list the zero-momentum energies  $E_\tau(0)$  and chiral splitting constants  $\tilde{B}_\tau$  for the  $C_2(y)$ -odd levels  $\tau = 1_{01}$  and  $\tau = 1_{10}$ .

To put the results in context, consider the physical parameters of current nanodroplet experiments, together with the hydrogen peroxide results. Ignoring finite-size effects, the thermal momentum distribution is expected

TABLE I: Results for HOOH.

$r_0$	$\tilde{A}$	$E_{1_{01}}(0)$	$\tilde{B}_{1_{01}}$	$E_{1_{10}}(0)$	$\tilde{B}_{1_{10}}$
1.86	0.94	1.64	$-2 \times 10^{-4}$	9.68	$3.2 \times 10^{-3}$
2.47	0.89	1.61	$-2 \times 10^{-4}$	8.94	$4.0 \times 10^{-3}$
3.06	0.83	1.57	$-3 \times 10^{-4}$	8.28	$6.2 \times 10^{-3}$
3.63	0.76	1.52	$-5 \times 10^{-4}$	7.73	$8.1 \times 10^{-3}$
4.21	0.67	1.46	$-6 \times 10^{-4}$	7.35	$9.1 \times 10^{-3}$
4.78	0.59	1.38	$-5 \times 10^{-4}$	7.13	$8.6 \times 10^{-3}$
(Å)	( $\text{cm}^{-1}\text{-Å}^2$ )	( $\text{cm}^{-1}$ )	( $\text{cm}^{-1}\text{-Å}$ )	( $\text{cm}^{-1}$ )	( $\text{cm}^{-1}\text{-Å}$ )

TABLE II: Results for FOOF.

$r_0$	$\tilde{A}$	$E_{1_{01}}(0)$	$\tilde{B}_{1_{01}}$	$E_{1_{10}}(0)$	$\tilde{B}_{1_{10}}$
1.97	0.46	0.31	$3 \times 10^{-4}$	0.83	$-5 \times 10^{-4}$
2.68	0.42	0.29	$2 \times 10^{-4}$	0.36	$-2 \times 10^{-4}$
3.32	0.43	0.30	$2 \times 10^{-4}$	0.81	$-6 \times 10^{-4}$
3.93	0.40	0.29	$2 \times 10^{-4}$	0.80	$-6 \times 10^{-4}$
4.53	0.37	0.28	$2 \times 10^{-4}$	0.78	$-6 \times 10^{-4}$
5.13	0.34	0.27	$2 \times 10^{-4}$	0.77	$-6 \times 10^{-4}$
(Å)	( $\text{cm}^{-1}\text{-Å}^2$ )	( $\text{cm}^{-1}$ )	( $\text{cm}^{-1}\text{-Å}$ )	( $\text{cm}^{-1}$ )	( $\text{cm}^{-1}\text{-Å}$ )

to be Maxwellian, i.e.  $dP/dk = Ck^2 \exp\left(-\frac{1}{2}\tilde{A}k^2/T\right)$ . The nanodroplet temperature is  $T = 0.4$  K. This corresponds to a typical thermal momentum of  $k_{rms} = 1 \text{ Å}^{-1}$  for HOOH. The ground-state momentum  $k_0$ , on the other hand, is only about  $0.01 \text{ Å}^{-1}$ , and is completely overwhelmed by thermal fluctuations. The  $\tau = 1_{01}$  and

## V. DISCUSSION

In this paper we have presented a classical model for the behavior of a molecule immersed in superfluid; and we have shown that the quantized version of the model has interesting features which should be, under certain conditions, spectroscopically detectable. In particular, chiral molecules can act as “quantum propellers,” coupling linear and angular momenta via their interaction with the superfluid medium, and this leads to a characteristic splitting of spectral lines. Our model simplifies the superfluid dynamics greatly, which presumably affects the quantitative accuracy of our results. We will conclude by discussing possible remedies for the shortcomings of our model.

One important physical effect that we have ignored is the formation of structured shells of helium atoms around a solvated impurity, which leads to a nonuniform fluid density. The model can be naturally extended to include this, by allowing the fluid density  $\rho_f$  to vary spatially, while maintaining a time-independent profile in the body frame. This approach has been used by other authors to estimate the superfluid-induced increase

$\tau = 1_{10}$  energy levels will each acquire fine structure by splitting into three evenly spaced sublevels with different values of  $M$ ; we estimate the spacing for these two sets of sublevels to be  $2\text{-}5 \times 10^{-4} \text{ cm}^{-1}$  and  $3\text{-}8 \times 10^{-3} \text{ cm}^{-1}$  respectively. Moreover, the center level ( $M = 0$ ) in each triplet is sharp, while the wings ( $M = \pm 1$ ) are broadened by the thermal spread in momentum. Because the experimental linewidth for rovibrational transitions is small, on the order of  $0.01 \text{ cm}^{-1}$ , we expect this fine structure to be nearly resolvable in the  $1_{01} \rightarrow 1_{10}$  absorption line for HOOH. If resolved, the line would appear as a sharp central peak, with broader peaks symmetrically placed on either side, at  $\pm 0.003 - 0.008 \text{ cm}^{-1}$ .

More generally, the resolvable fine structure of the absorption line for a dipole transition  $\tau_a \rightarrow \tau_b$  will depend on the relative values of  $k\tilde{B}_a$ ,  $k\tilde{B}_b$ , and the natural linewidth  $\Gamma$ . There may be three peaks (if  $k\tilde{B}_b \gg \Gamma \gg k\tilde{B}_b - k\tilde{B}_a$ ),  $2J_a + 1$  peaks (if  $k\tilde{B}_b - k\tilde{B}_a \gg \Gamma \gg k\tilde{B}_b$ ),  $3(2J_a + 1)$  peaks (if  $k\tilde{B}_b$  and  $k\tilde{B}_b - k\tilde{B}_a \gg \Gamma$ ), or more complicated possibilities when some peaks overlap. For the  $1_{01} \rightarrow 1_{10}$  transition in hydrogen peroxide, our theory predicts that the initial level spacing is very small, while the final level spacing is approximately resolvable, for typical thermal values of  $k$ . The expected line shape for this scenario is schematically depicted in Figure 3. There are three peaks, corresponding to the three possible final values of  $M$ . The central peak has the natural linewidth, since the  $M = 0$  energy has no first-order dependence on  $k$ , while the  $M = \pm 1$  wings are thermally broadened.

in the moments of inertia of linear or highly symmetric molecules [9, 11, 12]. The effect of a nonuniform density can be dramatic. For instance,  $\text{SF}_6$  has  $I = 180 \text{ amu}\text{-Å}^2$  in vacuum, which increases by  $\Delta I = 310 \text{ amu}\text{-Å}^2$  when the molecule is immersed in a helium droplet. The model presented here gives  $\Delta I < 25 \text{ amu}\text{-Å}^2$ , an order of magnitude too small, confirming the assessment by other authors that a rotating ellipsoid model can seriously underestimate  $\Delta I$  [11, 12]. By contrast, a calculation using a nonuniform density predicts  $\Delta I = 170 \text{ amu}\text{-Å}^2$ , which is more than half of the experimental value [11]. The comparison demonstrates that a rigid body with solvation shells attached drags more mass when it moves than one without them. It is tempting to speculate that the calculated chiral splitting constants  $\tilde{B}_\tau$  will also increase when a nonuniform density is allowed; but this may not be the case, for two reasons. First, since the off-diagonal Hamiltonian matrix  $\hat{\beta}$  is equal to  $-\hat{M}^{-1}\hat{G}\hat{I}^{-1}$  to lowest order in  $\hat{G}$ , increases in the rotational-translational coupling tensor are counteracted by corresponding increases in the hydrodynamic mass and inertia tensors. Second, attaching solvation shells to the immersed body simply builds a larger rigid body, to some extent, and the con-

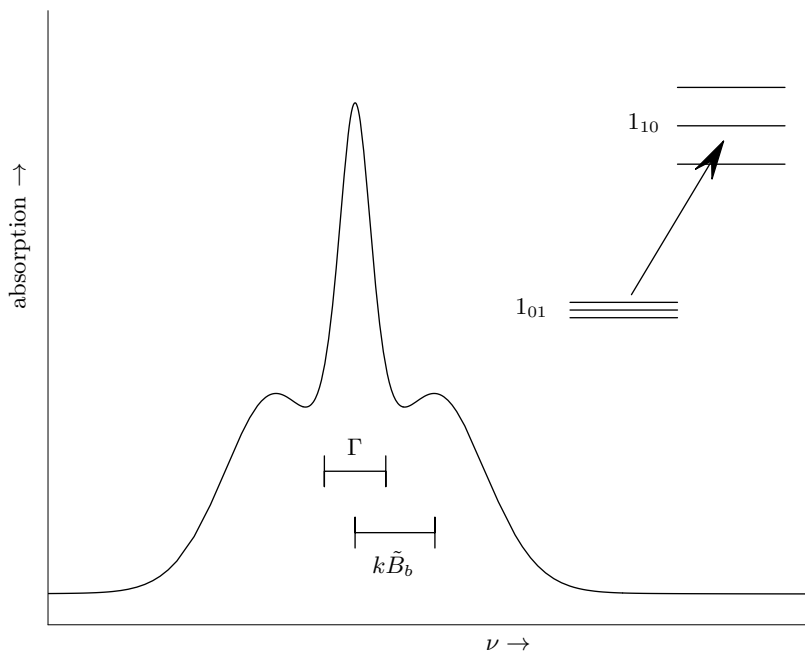


FIG. 3: Schematic representation of the predicted  $1_{01} \rightarrow 1_{10}$  absorption line in hydrogen peroxide. The strength of absorption is plotted as a function of the photon wavenumber,  $\nu$ .

stants  $\tilde{B}_\tau$  always vanish for a rigid body. Therefore, while allowing a nonuniform fluid density may alter our results, it is difficult to predict the outcome without performing a full calculation.

By studying the dynamics of immersed molecules in bulk superfluid, we have ignored the finite-size effects associated with immersion in a cluster or droplet. Our approach can be extended to handle reasonably large droplets with no fundamental difficulties. Lehmann has carried out a related calculation for the case of a linear molecule in a spherical droplet, taking into account the hydrodynamic effects which are present for an elliptical molecular surface (the modification of the rotational constants and the  $\hat{\alpha}$  matrix, in our notation), together with the effective interactions between the molecule and the droplet surface [10]. It would be interesting to extend the current work along similar lines. We expect that such an extension would lead to results qualitatively similar to those presented here. Because parity is a good symmetry for a superfluid droplet, as it is for bulk superfluid, parity would still be broken by the addition of a chiral impurity molecule, and this would manifest itself in a characteristic splitting of the rotational spectrum.

Microscopic details of the superfluid structure are also neglected by a continuum hydrodynamic approach. These details are better treated by path-integral and diffusion Monte Carlo methods, which have proven successful in predicting the rotational constants of immersed molecules [9]. It is likely that the hydrodynamic mass and rotational-translational tensors described here can also be extracted from such calculations, and this information would be a useful complement to the hydrody-

namic results. Monte Carlo methods could also be used to address another neglected phenomenon: the quantum-mechanical tunnelling between left-handed and right-handed forms of a chiral molecule. This may play a pronounced role in hydrogen peroxide, where the torsional ground state (a symmetric superposition of left- and right-handed forms) is  $11 \text{ cm}^{-1}$  below the first (antisymmetric) excited state [13]. Because the splitting is so large, comparable even to the rotational level spacing, the enantiomers are strongly mixed, making questionable our rigid-body treatment of the molecule. We expect the surrounding superfluid to suppress tunnelling, but a detailed calculation, without the assumption of rigidity, is needed for a quantitative assessment. (Some experimental support is provided by the work of Nauta and Miller, who studied immersed HF dimers; they found that the barrier to interchange tunnelling was raised significantly by the presence of the superfluid [14].) The main difficulty in applying Monte Carlo methods would be finite-size effects: since translational symmetry is strongly broken in small droplets, while rotational symmetry is preserved, the finite-size corrections to  $\hat{M}$  and  $\hat{G}$  are presumably more drastic than those to  $\hat{I}$ . A number of other microscopic techniques have been applied to molecular impurities in superfluid droplets (see Ref. [9] for a recent review), such as density functional theory, and these more elaborate methods may also be applicable to the phenomena we have described.

Finally, experimental data would be extraordinarily useful in refining the current model. The spectroscopic signatures we have described should be present for any chiral molecule, but not all candidate molecules will have



the large splitting constants necessary to resolve the fine structure. Nanodroplet experiments have been conducted using many different species of impurity molecule; Ref. [4] contains an exhaustive list. However, almost none of the studied molecules are chiral, so it is not surprising that no quantum propeller has yet been seen. We have suggested hydrogen peroxide (HOOH) as one strong candidate. Ideally, the present paper will provide sufficient impetus for more detailed investigations, both theoretical and experimental.

### Acknowledgments

This work was funded by a Department of Education GAANN Fellowship, No. P200A970615.

### APPENDIX A: CALCULATION OF FLUID TENSORS

For approximately spherical surfaces, it is possible to calculate the hydrodynamic mass, rotational-translational coupling, and inertia tensors as perturbation series in the deviation from sphericity. Consider a surface at  $r_s(\theta, \phi) = r_0(1 + \epsilon(\theta, \phi))$ . The surface normal times the area element is

$$\frac{\mathbf{n}da}{r_0^2 d^2\Omega} = (1 + \epsilon)(\mathbf{e}_r + i(\mathbf{e}_r \times \mathbf{J})) (1 + \epsilon), \quad (\text{A1})$$

where

$$\mathbf{J} \equiv i\mathbf{e}_\theta \frac{1}{\sin\theta} \frac{\partial}{\partial\phi} - i\mathbf{e}_\phi \frac{\partial}{\partial\theta} \quad (\text{A2})$$

is the usual vector of first-order differential operators on the sphere. For any scalar function  $\Phi$ ,

$$\nabla\Phi \cdot \frac{\mathbf{n}da}{r_0^2 d^2\Omega} = (1 + \epsilon)^2 \frac{\partial\Phi}{\partial r} + \frac{1}{r_0} \mathbf{J}\Phi \cdot \mathbf{J}\epsilon, \quad (\text{A3})$$

with derivatives evaluated at  $r = r_s$ . Applying this to Eq. (5a) for the translational response function  $\psi_\mu$  yields

$$\frac{\partial\psi_\mu}{\partial r} = n_\mu - \frac{1}{r_0(1 + \epsilon)^2} \mathbf{J}\psi_\mu \cdot \mathbf{J}\epsilon + \frac{1}{1 + \epsilon} i\epsilon_{\mu\nu\lambda} n_\nu (\mathbf{J}\epsilon)_\lambda, \quad (\text{A4})$$

where  $n_\mu = \mathbf{e}_\mu \cdot \mathbf{e}_r$ , and with derivatives evaluated at  $r = r_s$ . If  $\psi_\mu$  is expanded in orders of  $\epsilon$ , as  $\psi_\mu = \psi_\mu^{(0)} + \psi_\mu^{(1)} + \dots$ , and functions evaluated at  $r_s$  are expanded in Taylor series around  $r_0$ , then Eq. (A4) gives a single equation at each order in  $\epsilon$ :

$$\frac{\partial\psi_\mu^{(0)}}{\partial r} = n_\mu, \quad (\text{A5a})$$

$$\frac{\partial\psi_\mu^{(1)}}{\partial r} + r_0\epsilon \frac{\partial^2\psi_\mu^{(0)}}{\partial r^2} = -\frac{1}{r_0} \mathbf{J}\psi_\mu^{(0)} \cdot \mathbf{J}\epsilon + i\epsilon_{\mu\nu\lambda} n_\nu (\mathbf{J}\epsilon)_\lambda, \quad (\text{A5b})$$

and so forth, where now all derivatives are evaluated at  $r = r_0$ . Moreover,  $\nabla^2\psi_\mu^{(n)} = 0$  and  $|\nabla\psi_\mu^{(n)}(\mathbf{x})| \rightarrow 0$  as  $|\mathbf{x}| \rightarrow \infty$  for each  $n$ . The zeroth-order equation can be solved for  $\psi_\mu^{(0)}$ , and in general the equation of order  $\epsilon^n$  can be solved for  $\psi_\mu^{(n)}$  once all the  $\psi_\mu^{(m)}$  with  $m < n$  are known. Therefore  $\psi_\mu$  can be calculated to any order in  $\epsilon$ , though the process rapidly becomes tedious. Similarly, the rotational response function  $\chi_\mu$  satisfies the simpler equation

$$\frac{\partial\chi_\mu}{\partial r} = -ir_0(\mathbf{J}\epsilon)_\mu - \frac{1}{r_0(1 + \epsilon)^2} \mathbf{J}\chi_\mu \cdot \mathbf{J}\epsilon \quad (\text{A6})$$

at  $r = r_s$ , which follows from Eq. (5b); and this can be used to find  $\chi_\mu$  to any order in  $\epsilon$ , in exactly the same way.

Once the response functions are in hand, Eqs. (10) can be evaluated to obtain the fluid tensors. This, too, is done order-by-order in  $\epsilon$ . The results are best expressed as angular averages. Through second order in  $\epsilon$ ,

$$\frac{\delta M_{\mu\nu}}{4\pi\rho_f r_0^3} = \frac{1}{6} \delta_{\mu\nu} + \left\langle \left( -\frac{9}{4} n_\mu n_\nu + \frac{5}{4} \delta_{\mu\nu} \right) \epsilon \right\rangle - \left\langle \psi_\mu^{(1)} \frac{\partial\psi_\nu^{(1)}}{\partial r} \right\rangle, \quad (\text{A7a})$$

$$\frac{\delta G_{\mu\nu}}{4\pi\rho_f r_0^4} = \frac{1}{2} \epsilon_{\mu\nu\lambda} \langle n_\lambda \epsilon \rangle - \left\langle \psi_\mu^{(1)} \frac{\partial\chi_\nu^{(1)}}{\partial r} \right\rangle, \quad (\text{A7b})$$

$$\frac{\delta I_{\mu\nu}}{4\pi\rho_f r_0^5} = - \left\langle \chi_\mu^{(1)} \frac{\partial\chi_\nu^{(1)}}{\partial r} \right\rangle, \quad (\text{A7c})$$

where  $\langle f \rangle \equiv \frac{1}{4\pi} \int f(\Omega) d^2\Omega$ , and functions are evaluated at  $r_0$ . Here the first-order fields  $\psi_\mu^{(1)}$  and  $\chi_\mu^{(1)}$  are determined by their radial derivatives at  $r_0$ , which are

$$\begin{aligned} \frac{\partial\psi_\mu^{(1)}}{\partial r} &= -\frac{3}{2} i\epsilon_{\mu\nu\lambda} n_\nu (\mathbf{J}\epsilon)_\lambda - 3n_\mu \epsilon, \\ \frac{\partial\chi_\mu^{(1)}}{\partial r} &= -i(\mathbf{J}\epsilon)_\mu. \end{aligned} \quad (\text{A8})$$

Note that  $\delta\hat{G}$  is antisymmetric to first order. Because the antisymmetric part of  $\hat{G}$  is eliminated by the correct choice of body origin, it was necessary to carry the calculation of  $\delta\hat{G}$  to second order to obtain nontrivial rotational-translational coupling.

- 
- [1] For the published version of this article, see: M. J. Quist and V. Elser, *J. Chem. Phys.* **117**, 3878 (2002). Copyright 2002 by the American Institute of Physics.
- [2] S. Grebenev, B. Sartakov, J. P. Toennies, and A. F. Vilesov, *Science* **289**, 1532 (2000).
- [3] S. Grebenev, M. Havenith, F. Madeja, J. P. Toennies, and A. F. Vilesov, *J. Chem. Phys.* **113**, 9060 (2000).
- [4] C. Callegari, K. K. Lehmann, R. Schmied, and G. Scoles, *J. Chem. Phys.* **115**, 10090 (2001).
- [5] Sir Horace Lamb, *Hydrodynamics* (Cambridge University Press, New York, 1993), 6th ed.
- [6] D. M. Brink and G. R. Satchler, *Angular Momentum* (Clarendon Press, Oxford, 1993), 3rd ed.
- [7] A. Bondi, *J. Phys. Chem.* **68**, 441 (1964).
- [8] R. H. Jackson, *J. Chem. Soc.*, 4585 (1962).
- [9] Y. Kwon, P. Huang, M. V. Patel, D. Blume, and K. B. Whaley, *J. Chem. Phys.* **113**, 6469 (2000).
- [10] K. K. Lehmann, *Mol. Phys.* **97**, 645 (1999).
- [11] K. K. Lehmann and C. Callegari, e-print: physics/0109009.
- [12] C. Callegari, A. Conjusteau, I. Reinhard, K. K. Lehmann, G. Scoles, and F. Dalfovo, *Phys. Rev. Lett.* **83**, 5058 (1999).
- [13] P. Helminger, W. Bowman, and F. De Lucia, *J. Mol. Spectrosc.* **171**, 91 (1981).
- [14] K. Nauta and R. E. Miller, *J. Chem. Phys.* **113**, 10158 (2000).